

Chapter 2

Periodically modulated dispersion, and dispersion management: basic results for solitons

2.1 Introduction to the topic

Dispersion management (DM) is a name commonly adopted in the literature for the model based on the NLS equation (1.48) with a constant nonlinearity coefficient γ and the sign-changing GVD coefficient β , modulated along the propagation distance z as per Eq. (1.49). As explained in Introduction, the transmission of quasi-soliton signals, alias *return-to-zero* (RZ) pulses, in the DM model is an issue of fundamental importance to fiber-optic telecommunications. It should be stressed that, unlike many other nonlinear systems with periodic management, where the results have thus far been chiefly theoretical, the DM solitons in fiber-optic telecommunication links were studied in the experiment in detail, see, e.g., paper [38].

Most theoretical works which studied the soliton transmission in the DM model relied on direct numerical simulations. As concerns analytical approaches, two most significant ones are based on the variational approximation (VA), and on integral equations. Actually, both methods assume that the nonlinearity in the model is weak enough, so that, in the zero-order approximation, the RZ pulse may be approximated by the expression (1.51), which is an exact solution to the linear version of Eq. (1.48).

The integral formalism for the DM solitons was worked out by Gabitov and Turitsyn [69] and Ablowitz and Biondini [9] (see also paper [138]). It is based on an idea that, in the linear limit, a general solution to equation (1.48) can be searched for by

means of the Fourier transform as

$$u(z, \tau) = \frac{1}{2\pi} \int_{-\infty}^{+\infty} e^{-i\omega\tau} \hat{u}(z, \omega) d\omega. \quad (2.1)$$

Substituting this representation in the linear version of Eq. (1.48), one immediately derives an evolution equation for the Fourier transform:

$$\frac{d\hat{u}}{dz} = \frac{i}{2} \omega^2 \beta(z) \hat{u}, \quad (2.2)$$

a solution to which is obvious,

$$\hat{u}(z, \omega) = \hat{u}(0, \omega) \exp\left(\frac{i}{2} \omega^2 B(z)\right), \quad (2.3)$$

where $B(z)$ is the *accumulated dispersion*, defined as per Eq. (1.52).

If the nonlinearity is taken into regard, the wave field can still be represented in the form of Eq. (2.1), but then the nonlinear term in Eq. (1.48), after the substitution of the Fourier representation, will add a cubic integral term to the evolution equation (2.2). Various results can then be obtained from the analysis of the nonlinear integral equation.

Similar to the integral formalism, the VA also makes use of the linear limit of Eq. (1.48); however, it starts not with the general linear superposition (1.51), but rather with the fundamental solution (1.51). The general idea of the VA is that, after the introduction of the weak nonlinearity, the Gaussian wave form (1.51) may be an adequate *ansatz* for the solution, assuming that its constant parameters may become slowly varying functions of z ; the main objective of the variational technique is to derive equations governing slow evolution of the parameters. In this chapter, the variational approach will be presented following, chiefly, paper [100].

Besides the model with the DM map (1.49), it is also interesting to consider a system with the harmonic modulation of the GVD coefficient,

$$\beta(z) = -(1 + \varepsilon \sin z), \quad (2.4)$$

where the PAD is normalized to be -1 , and the modulation period is scaled to be 2π . Although the sinusoidal modulation is not a realistic assumption for fiber-optic telecommunications, the model is of interest in its own right, as it may predict quite interesting results even for relatively small values of the modulation amplitude ε , when the local GVD coefficient (2.4) does not change its sign, remaining always negative (i.e., corresponding to the anomalous GVD). In fact, nontrivial results (such as splitting of a soliton into two, see below) may be generated by resonances between internal vibrations of a perturbed soliton, and the periodic modulation defined by Eq. (2.4).

In this chapter, the analysis will be performed first for the model (2.4), and then for the one (1.49). The VA (combined with direct simulations) will be used in both cases, but the results will be very different, due to the fundamental difference between the two types of the periodic modulation.

2.2 The model with the harmonic modulation of the local dispersion

In the case of the harmonic modulation (2.4), the NLS equation (1.5) takes the form

$$iu_z + \frac{1}{2} (1 + \varepsilon \sin z) u_{\tau\tau} + |u|^2 u = 0, \quad (2.5)$$

where the normalization $\gamma = 1$ is adopted. This model was introduced in 1993 in paper [110], with the intention to study possible resonances in it. In that first work, only the VA was used, without direct simulations. An important contribution to the analysis of the model was later made by Abdullaev and Caputo [3], and direct comparison of the predictions of the VA with direct simulations, which reveal effects that the VA could not predict, was reported in paper [76].

2.2.1 Variational equations

The application of the VA to the soliton in the model (2.5) was described many times and summarized in review [104], therefore here it will be presented in a brief form. The VA assumes the ansatz which mimics the exact NLS soliton solution (1.13), but with arbitrary amplitude A , temporal width a , and phase ϕ ; in addition, it is assumed that the nonstationary soliton may have *chirp*, i.e., a parabolic phase profile across the pulse, with a real coefficient b in front of it:

$$u_{\text{ansatz}}(z, \tau) = A(z) \operatorname{sech} \left(\frac{\tau}{a(z)} \right) \exp [i\phi(z) + ib(z)\tau^2]. \quad (2.6)$$

All the free parameters in the ansatz are allowed to be functions of the evolutionary variable z , the first objective being to derive a system of evolution equations for them. This is done using the fact that the NLS equation can be derived, in the form of $\delta S / \delta u^* = 0$, from the *action functional* $S\{u, u^*\}$, where $\delta / \delta u^*$ is the symbol for the variational derivative. The action is represented in the form of $S = \int L dz$, where L is a *Lagrangian*, that has its own integral form, $L = \int_{-\infty}^{+\infty} \mathcal{L} d\tau$, with a *Lagrangian density* \mathcal{L} , which must be real. For the NLS equation (1.5), the latter is

$$\mathcal{L} = \frac{i}{2} (u^* u_z - u u_z^*) + \frac{1}{2} \beta(z) |u_\tau|^2 + \frac{1}{2} \gamma |u|^4. \quad (2.7)$$

The insertion of the ansatz (2.6) into the Lagrangian and analytical integration in τ yields the corresponding effective Lagrangian, as a function of the variational parameters and their z -derivatives (denoted by the prime),

$$L_{\text{eff}}^{(\text{NLS})} = -2A^2 a \phi' - \frac{\pi^2}{6} A^2 a^3 b' + \frac{1}{3} \beta(z) \frac{A^2}{a} - \frac{\pi^2}{3} D A^2 a^3 b^2 + \frac{2}{3} \gamma A^4 a. \quad (2.8)$$

A standard set of the variational (Euler-Lagrange) equations follows from the effective Lagrangian,

$$\begin{aligned} \frac{d}{dz} \frac{\partial L_{\text{eff}}^{(\text{NLS})}}{\partial \phi'} &= 0, \quad \frac{d}{dz} \frac{\partial L_{\text{eff}}^{(\text{NLS})}}{\partial b'} - \frac{\partial L_{\text{eff}}^{(\text{NLS})}}{\partial b} = 0, \\ \frac{\partial L_{\text{eff}}^{(\text{NLS})}}{\partial a} &= \frac{\partial L_{\text{eff}}^{(\text{NLS})}}{\partial A} = 0. \end{aligned} \quad (2.9)$$

After straightforward manipulations, these equations can be cast in the following form:

$$\frac{d}{dz} (A^2 a) = 0, \quad (2.10)$$

$$b = -(2\beta(z)a)^{-1} \frac{da}{dz}, \quad (2.11)$$

$$\frac{d}{dz} \left[(-\beta(z))^{-1} \frac{da}{dz} \right] = -\frac{\partial U_{\text{eff}}(a)}{\partial a}, \quad (2.12)$$

$$U_{\text{eff}}(a) \equiv -\frac{2}{\pi^2} (\beta a^{-2} + 2\gamma E a^{-1}), \quad E \equiv A^2 a, \quad (2.13)$$

supplemented by a separate equation for the phase,

$$\frac{d\phi}{dz} = \frac{\pi^2}{12} a^2 \left[\frac{db}{dz} - 2\beta(z)b^2 \right] - \frac{1}{6} \frac{\beta(z)}{a^2} - \frac{2}{3} \gamma A^2. \quad (2.14)$$

Equation (2.10) implies the existence of the dynamical invariant $E \equiv A^2 a$. The conservation of this quantity is a straightforward manifestation of the conservation of energy (1.9) in the full NLS equation. Indeed, the substitution of the ansatz (2.6) into Eq. (1.9) yields $E = A^2 a$. Equation (2.11) shows that the intrinsic chirp of the soliton is generated by its deformation (change of the width).

Equations (2.12) and (2.13) demonstrate that the evolution of the soliton's width can be represented as a motion of a Newtonian particle with a variable mass $-1/\beta(z)$ and a coordinate $a(z)$ in the potential well $U_{\text{eff}}(a)$, while the propagation distance z plays the role of time. For the case when β is a negative constant, the potential is shown in Fig. 2.1. In this case, the bottom of the potential well corresponds to an equilibrium position at

$$a = a_{\text{eq}} \equiv -\frac{\beta}{\gamma E}. \quad (2.15)$$

Comparison with the expression (1.13) shows that the ansatz (2.6) with $a = a_{\text{eq}}$ exactly coincides with the unperturbed soliton solution.

In the case of constant β , Eq. (2.12) with the potential (2.13) is tantamount to the equation of motion for the radial variable r in the classical Kepler's problem (motion

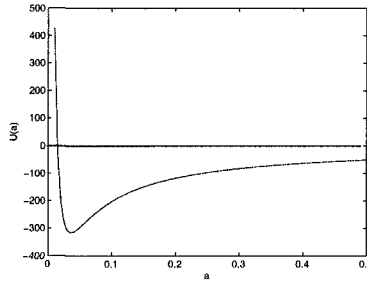


Figure 2.1: The effective potential (2.13) for $\beta = -1$, $\gamma E = 4\pi^2$.

of a particle in the gravitational field with the potential $-1/r$) [3]. Accordingly, exact solutions can be found in a parametric form,

$$a = -\left(\frac{2E}{\pi^2 H}\right) \left(1 - \sqrt{1 - \frac{\pi^2 |H|}{2E^2}} \cos \xi\right), \quad \left(\frac{\pi^2 |H|^{3/2}}{\sqrt{2E}}\right) z = \xi - \sqrt{1 - \frac{\pi^2 |H|}{2E^2}} \sin \xi, \quad (2.16)$$

where it was set $-\beta = \gamma = 1$, ξ is an auxiliary dynamical variable, and H is the value of the Hamiltonian of the equivalent Kepler's problem, that takes values in the interval $-(2/\pi^2) E^2 < H < 0$ (the minimum value of H corresponds to the equilibrium position (2.15) at the well's bottom). The frequency of the oscillatory solution $a(z)$, as given by Eqs. (2.16) is

$$K = \frac{\pi^2 |H|^{3/2}}{\sqrt{2E}}. \quad (2.17)$$

It takes the maximum value

$$K_0 = 2E^2/\pi \quad (2.18)$$

at $H = -(2/\pi^2) E^2$, which corresponds to small oscillations near the bottom of the potential well.

2.2.2 Soliton dynamics in the model with the harmonic modulation

Predictions of the variational approximation

As was mentioned above, in the case of the harmonic periodic modulation of the local GVD coefficient, such as in Eq. (2.5), one may expect resonances between intrinsic vibrations of the free soliton, which are described, within the framework of the VA, by the solution (2.16), and external modulation of the GVD coefficient. Possible resonances can be studied analytically in the case of shallow modulation, $\varepsilon \ll 1$, by expanding equation (2.12) around the equilibrium position (2.15), and retaining quadratic and cubic nonlinear terms in the expansion. The fundamental resonance corresponds to the

case when the (spatial) frequency K_0 of free small oscillations near the equilibrium position, given by Eq. (2.18), is close to the spatial modulation frequency, which is 1 in Eq. (2.5). In other words, varying the initial soliton's energy E , one may expect that the *fundamental resonance* occurs in a vicinity of the value $E_{\text{fundam}} = \sqrt{\pi}/2 \approx 1.25$. Further, the first *subharmonic resonance*, corresponding to $2K_0$ close to 1, and the *second-order resonance*, which takes place for K_0 close to 2, are expected around $E_{\text{subharm}} = \sqrt{\pi}/2 \approx 0.87$ and $E_{\text{second}} = \sqrt{\pi} \approx 1.77$, respectively.

Actual predictions of the VA should be obtained by from numerical simulations of Eq. ((2.12) with $\beta(z) = -(1 + \varepsilon \sin z)$. In particular, a solution with $a(z) \rightarrow \infty$ at $z \rightarrow \infty$ is interpreted as destruction of the soliton, as it becomes infinitely broad. In fact, this implies decay of the soliton into radiation.

The simulations performed in work [110] have demonstrated that, in an interval of values of the soliton's energies E which covers both the above-mentioned first subharmonic and second-order resonances, oscillations of $a(z)$ driven by the sinusoidal modulation of $\beta(z)$ are anharmonic but still periodic at very small values of ε , typically $\varepsilon \sim 0.01$. With the increase of the modulation depth ε , the oscillations become nonperiodic at $\varepsilon \sim 0.05$, and apparently chaotic at ε closer to 0.20. Finally, a critical value ε_{cr} can be found such that, at ε slightly larger than ε_{cr} , $a(z)$ performs a large number of irregular oscillations inside the potential wall, and then suddenly gets kicked out from the trapped state and escapes to infinity, as shown in a typical example in Fig. 2.2. The escape actually implies indefinite spreading out of the pulse, i.e., its eventual decay into radiation. In all the cases considered (with different values of the energy E), the critical modulation amplitude takes values in the interval

$$0.20 < \varepsilon_{\text{cr}} < 0.25. \quad (2.19)$$

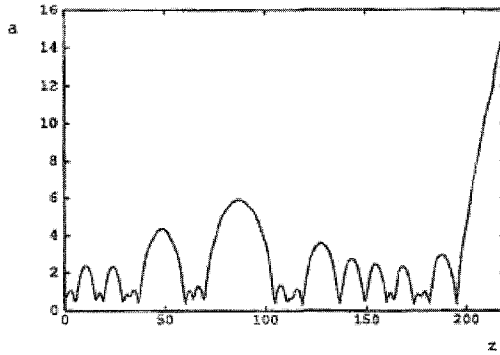


Figure 2.2: An example of the destruction of the soliton by a relatively weak harmonic modulation of the group-velocity-dispersion coefficient, $\beta(z) = -(1 + 0.25 \sin z)$, as predicted by numerical simulations of the variational equation (2.12). In this case, the energy is taken as $E = \sqrt{\pi} \approx 1.77$, which corresponds to the second-order resonance in small-amplitude driven oscillations near the bottom of the potential well (see the text). The width of the soliton, $a(z)$, performs a large number of irregular oscillations in the well, but finally escapes, which implies the decay of the soliton into radiation waves.

In the case when the modulation amplitude ε is small, the rate of direct emission of radiation by the soliton (obviously, this effect is beyond the scope of the VA) can be calculated by means of the perturbation theory [4]; however, this process does not play a crucial role in the destruction of the soliton.

Numerical results

The predictions produced by VA for the soliton in the NLS equation (2.5) with the sinusoidally modulated local GVD were compared with results of direct simulations of the equation in work [76]. Results of the simulations are summarized in Fig. 2.3. Two gross feature of this diagram roughly comply with predictions of the VA. Firstly, the destruction of the soliton may take place if the modulation amplitude exceeds a critical value, which varies, essentially, within an interval $0.15 < \varepsilon_{cr} < 0.20$, that should be compared to interval (2.19) predicted by VA. Secondly, the destruction of the soliton actually takes place, for ε not too large, if the initial squared soliton's energy E^2 exceeds a minimum value E_{min}^2 varying between 1.8 and 2.0, which may be compared to the above-mentioned value $E_{fundam}^2 = \pi/2$ that gives rise to the fundamental resonance between small vibrations of the perturbed soliton and the periodic modulation of the local GVD in Eq. (2.5).

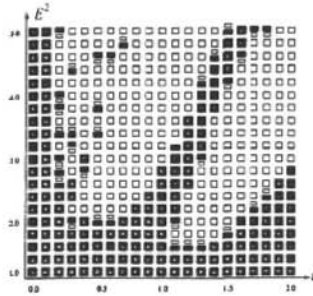


Figure 2.3: The phase diagram in the parametric plane (ε, E^2) for solitons in Eq. (2.5). The filled and unfilled rectangles correspond, respectively, to stable and splitting solitons.

The most essential difference between the assumptions on which the VA was based and numerical results is that the fundamental mode of the soliton destruction under the action of the sinusoidally modulated dispersion is not decay into radiation, but *splitting* of the soliton into two apparently stable secondary solitons (which is accompanied by emission of a considerable amount of radiation). A typical example of the splitting is displayed in Fig. 2.4. Obviously, the ansatz (2.6) does not admit any splitting; nevertheless, basic characteristics of the destruction of the soliton, even if the actual destructions mode is different from the one postulated by the VA, are predicted by the approximation qualitatively and semi-quantitatively correctly.

Detailed inspection of the numerical results shows that, prior to the splitting, the soliton performs a number of irregular vibrations, which resembles the picture produced by the VA, cf. Fig. 2.2. As well as in that picture, the vibrational stage preced-

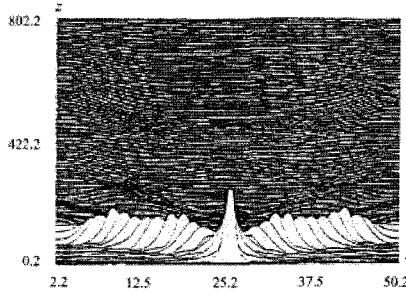


Figure 2.4: A typical example of the splitting of a fundamental soliton into two secondary ones in the NLS equation (2.5) with the sinusoidal modulation of the local dispersion coefficient, for $\varepsilon = 0.3$ and $E^2 = 2.9$

ing the destruction of the soliton is quite long if the splitting takes place at ε that only slightly exceeds the corresponding critical value ε_{cr} .

The soliton stability diagram in the sinusoidally-modulated model (2.5), displayed in Fig. 2.3, has a number of other noteworthy features, such as a narrow “stability isthmus”, and a trend to restabilization of the soliton at large ε (note that for $\varepsilon > 1$, the local GVD coefficient in Eq. (2.5) becomes sign-changing). These features are observed in a parameter region where the VA cannot be used.

Essential additional results concerning the comparison between the VA and direct simulations in the same model were reported, on the basis of direct simulations, by Abdullaev and Caputo [3]. They have also found that the destruction of the soliton takes place via its splitting into two secondary ones, and demonstrated that agreement between the VA and direct simulations of small intrinsic vibrations of the soliton is fairly good as long as the vibration frequency K_0 , see Eq. (2.18), remains *smaller* than the external modulation frequency (recall it is set to be 1 in Eq. (2.5)). At $K_0 \gtrsim 1$, intensive emission of radiation takes place (even without complete destruction of the soliton), which, naturally, strongly affects the agreement with the VA, as the approximation completely disregarded the radiation component of the field. Another important numerical finding reported in work [3] is that, in cases when the variational and direct numerical result are generally close, a more subtle effect of the radiation loss is strong suppression of higher harmonics in the soliton’s internal vibrations, in comparison with the picture predicted by the VA.

2.3 Solitons in the model with dispersion management

This section deals with solitons in the practically important model of the long dispersion-compensated nonlinear fiber link based on Eqs. (1.48) and (1.49). For convenience, the equations are given here again:

$$iu_z - \frac{1}{2}\beta(z)u_{\tau\tau} + \gamma|u|^2u = 0, \quad (2.20)$$

$$\beta = \begin{cases} \beta_1 > 0, & \text{if } 0 < z < L_1, \\ \beta_2 < 0, & \text{if } L_1 < z < L_1 + L_2 \equiv L, \end{cases} \quad (2.21)$$

The concept of the dispersion management (DM) for solitons in dispersion-compensated systems which, in the simplest case, amount to the model based on Eqs. (2.20) and (2.21), was introduced nearly simultaneously in works by Knox, Forysiak, and Doran [95], Suzuki, Morita, Edagawa, Yamamoto, Taga, and Akiba [160], Nakazawa and Kubota [131], and Gabitov and Turitsyn [69]. The original motivation for the development of the DM technique for solitons was the necessity to suppress the *Gordon-Haus effect*, i.e., random jitter of the soliton's center due to its interaction with optical noise, which is accumulated in the fiber-optic link due to the spontaneous emission from the optical amplifiers (these are actually Erbium-doped segments of the fiber, periodically inserted into the link, with the objective to compensate the fiber loss). The dispersion-managed solitons were predicted (and found in the experiment) to have large energy, which helps to improve the noise-to-signal ratio. Indeed, it has been demonstrated that the DM technique is very efficient in stabilizing solitons against the random jitter. On the other hand, a problem for the use of solitons in the DM system is posed by interactions between them. As the DM solitons periodically expand and contract, they may tangibly overlap, through their “tails”, at the expansion stage, which leads to the increase of unwanted interaction between them. Besides their great significance to the applications, solitons in DM models have also drawn a great deal of attention as a subject of fundamental research. The account given below focuses chiefly on the latter point, although applied aspects are briefly considered too.

As explained below, the VA is a very natural tool to investigate the soliton dynamics in DM models. The presentation in this section will chiefly follow the approach elaborated in works [100] and [106] (the latter work applied the VA, in combination with direct simulations, to solitons in a model of *random DM*). In particular, the same normalization of parameters of the DM map (2.21) as in paper [100] is adopted here,

$$(\beta_1 - \beta_0) L_1 + (\beta_2 - \beta_0) L_2 = 0, |\beta_1 - \beta_0| L_1 = |\beta_2 - \beta_0| L_2 = 1, L \equiv L_1 + L_2 = 1, \quad (2.22)$$

which can be always imposed by means of an obvious rescaling (recall β_0 is the PAD defined as per Eq. (1.50)).

In the case of strong DM, when the nonlinear term in Eq. (2.20) may be treated as a small perturbation, the RZ Gaussian pulse (1.51), which is the exact solution in the linear limit, may be used as a natural variational ansatz, to take into regard effects of the weak nonlinearity. For convenience, the ansatz is written here again:

$$u_{\text{RZ}}(z, \tau) = \sqrt{\frac{P_0}{1 - 2iB(z)/W_0^2}} \exp\left(-\frac{\tau^2}{W^2(z)} - \frac{2iB(z)}{W_0^2 W^2(z)}\right), \quad (2.23)$$

$$B(z) \equiv B_0 + \int_0^z \beta(z') dz' \quad (2.24)$$

The PAD will also be treated as a small perturbation, as an intuitive assumption is that the weak nonlinearity and small PAD may effectively compensate each other,

supporting a robust RZ pulse (alias, DM soliton). An important dimensionless characteristic of the pulse (2.23) is its *dispersion-management strength*, which is defined as

$$S \equiv 1.443 \frac{|\beta_1| L_1 + |\beta_2| L_2}{W_0^2}. \quad (2.25)$$

The factor 1.443 appears here due to the use of the so-called FWHM (full-width-at-half-maximum) definition of the pulse's width, which is different from W_0 . According to the value of S , the DM schemes are usually categorized as *weak-DM*, *moderate-DM*, and *strong-DM* regimes – in the cases of, roughly, $S < 3$, $S \sim 3 - 4$, and $S > 4$, respectively.

The VA is based on the assumption that the arbitrary constants W_0 and B_0 in Eqs. (2.23) and (2.24) become slowly varying functions of z , if the weak nonlinearity is taken into regard. Additionally, the accumulated dispersion $B(z)$ is defined for the map (2.21) from which the PAD value β_0 is subtracted. The analysis presented in detail in paper [100] yields the following evolution equations for the slowly varying parameters:

$$\frac{dW_0}{dz} = -\sqrt{2} \frac{EW_0 B(z)}{W^3(z)}, \quad (2.26)$$

$$\frac{dB_0}{dz} = \beta_0 - \frac{E [4B^2(z) - W_0^4]}{2\sqrt{2} W^3(z)}, \quad (2.27)$$

where the function $W(z)$ is defined in Eq. (1.53). To derive these equations, the normalization (2.22) was used, and the energy of the pulse is defined as $E = P_0 \tau_0$ (recall that P_0 is peak power, i.e., maximum value of the squared amplitude, in expression (2.23)). In fact, E plays the role of a small parameter measuring the relative weakness of the nonlinearity in comparison with the local dispersion.

An issue of fundamental interest is to find conditions allowing for the *stationary transmission* of the pulse, i.e., a dynamical regime in which the parameters W_0 and B_0 return to their initial values after passing one DM period. Because, as it is seen from Eqs. (2.26) and (2.27), changes of W_0 and B_0 within one period are generally small, $\sim (\beta_0, E)$, in the first approximation one may insert unperturbed values of W_0 and B_0 into the right-hand sides of Eqs. (2.26) and (2.27), and impose the conditions that (recall that the DM period is 1 in the present notation)

$$\int_0^1 \frac{dW_0}{dz} dz = \int_0^1 \frac{dB_0}{dz} dz = 0. \quad (2.28)$$

After some analytical calculations, Eqs. (2.28) yield the following stationary-propagation conditions for the Gaussian pulse in an explicit form,

$$B_0 = \frac{1}{2}, \quad \beta_0 = \frac{\sqrt{2}}{4} E \tau_0^3 \left[\ln \left(\sqrt{1 + \frac{1}{W_0^4}} + \frac{1}{W_0^2} \right) - \frac{2}{\sqrt{W_0^4 + 1}} \right]. \quad (2.29)$$

The meaning of the condition $B_0 = 1/2$ is quite simple: it requires the pulse to have zero chirp at the midpoint of each fiber segment. The second condition (2.29) predicts that the DM soliton propagates steadily at anomalous PAD, $\beta_0 < 0$, provided that $W_0^2 > (W_0^2)_{\text{cr}} \approx 0.30$, at $\beta_0 = 0$ if $W_0^2 = (W_0^2)_{\text{cr}}$, and at *normal* PAD, $\beta_0 > 0$, if $(W_0^2)_{\text{min}} \approx 0.148 < W_0^2 < (W_0^2)_{\text{cr}}$. The latter case is very interesting, as the classical NLS soliton cannot exist at normal dispersion. Further analysis of Eq. (2.29) shows that, in this case, the solution exists in a limited interval of the normal-PAD values,

$$0 \leq \beta_0/E \leq (\beta_0/E)_{\text{max}} \approx 0.0127. \quad (2.30)$$

Inside this interval, Eq. (2.29) yields *two* different values of the minimum width W_0 for a given value of β_0/E , while in the anomalous-PAD region, W_0 is a uniquely defined function of β_0/E . In the case of the normal PAD, $\beta_0 > 0$, it can be concluded that the DM soliton corresponding to the larger value of W_0 is stable, while the one corresponding to smaller W_0 is unstable. The border between the stable and unstable solitons corresponds to $\beta_0/E = (\beta_0/E)_{\text{max}}$ (see Eq. (2.30)), and it is located at $W_0^2 = (W_0^2)_{\text{min}} \approx 0.148$ (i.e., all the stable and unstable solitons have, respectively, $W_0^2 > (W_0^2)_{\text{min}}$ and $W_0^2 < (W_0^2)_{\text{min}}$). The results concerning the stability of these two solitons were substantiated in a mathematically rigorous form in work [140].

Translating W_0^2 into the standard DM-strength parameter S according to Eq. (2.25), one concludes that the VA predicts the following:

- stable DM solitons at anomalous PAD if $S < S_{\text{cr}} \approx 4.79$;
- stable DM solitons at *zero* PAD if $S = S_{\text{cr}} \approx 4.79$;
- stable DM solitons at *normal* PAD if $4.79 < S < S_{\text{max}} \approx 9.75$;
- no stable DM soliton for $S > S_{\text{max}} \approx 9.75$.

The normalized power of the DM soliton, which is $P \equiv 4 \cdot 1.12P_0$ (the factor 1.12 is the ratio of the FWHM widths for the sech-shaped and Gaussian pulses) is shown vs. the DM strength, at several fixed values of PAD β_0 , as predicted by Eq. (2.29), in Fig. 2.5. A counterpart of the same dependence, obtained in work [31] from direct simulations of the underlying equation (2.20), is displayed in Fig. 2.6 (a typical example of the shape of the DM soliton, found from direct simulations, is displayed below in Fig. 2.10). In Fig. 2.5, the curves are shown only in the region of $S < 9.75$, where the solitons are expected to be stable. The curves in Fig. 2.6 corresponding to the normal PAD ($\beta_0 > 0$) terminate at points where the corresponding DM soliton becomes unstable.

As a matter of fact, Fig. 2.6 is the most fundamental and comprehensive characteristic of the family of the DM solitons. The comparison of Figs. 2.5 and 2.6 shows that the VA yields acceptable results for relatively small values of the soliton's power, where the underlying assumption, that the nonlinearity may be treated as a weak perturbation, is relevant. In particular, the VA-predicted critical value $S_{\text{cr}} \approx 4.79$ is different from but nevertheless reasonably close to the critical DM strength $S_{\text{cr}} \approx 4$ which direct simulations yield in the small-power limit. With the increase of power, numerically found

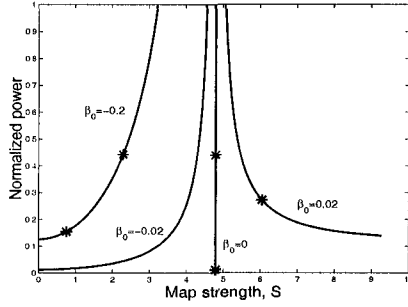


Figure 2.5: The peak power of the stable soliton in the DM system vs. the map strength S at different values of the path-average dispersion β_0 , as predicted by the variational approximation based on Eq. (2.29). Here and in the next figure, stars mark cases for which the corresponding model with *random DM* was investigated in detail, see section 2.4.

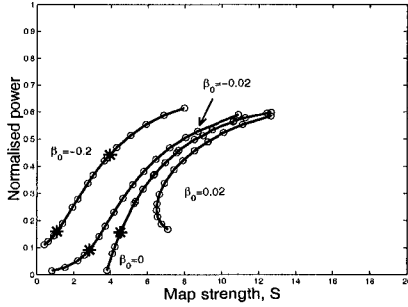


Figure 2.6: A counterpart of Fig. 2.5 obtained from direct numerical simulations of Eq. (2.20).

S_{cr} grows. It is also noteworthy that the value $S_{\text{max}} \approx 9.75$, predicted by the VA as the stability limit for the DM solitons, is indeed close to what is revealed by direct simulations for small powers, as seen in Fig. 2.6.

The DM soliton considered above is a fundamental one (i.e., it always keeps the single-peak shape). Higher-order DM solitons can be constructed too. Indeed, along with the expression (2.23), its τ -derivatives of all orders are also exact solutions to the linearized version of Eq. (2.20), and can be used as *ansätze* to generate an (approximate) higher-order soliton solutions in the weakly nonlinear case. In particular, an ansatz proportional to the first derivative of the Gaussian (2.23),

$$\left(u_{\text{RZ}}^{(\text{linear})}(z, \tau)\right)_{\text{odd}} = \sqrt{\frac{P_0}{1 - 2iB(z)/W_0^2}} \frac{\tau}{W^2(z)} \exp\left(-\frac{\tau^2}{W^2(z)} - \frac{2iB(z)}{W_0^2 W^2(z)}\right), \quad (2.31)$$

was used in work [137] to construct an odd (antisymmetric, as a function of τ) DM soliton. However, this soliton is unstable against even perturbations. Related to this

generalization is another technical approach to the description of the fundamental DM solitons and perturbations around them: an extended solution, including the perturbation, may be looked for starting from a linear combination of Hermite-Gauss functions (of τ) [167, 99]. In particular, this approach correctly reproduces the results of the VA.

2.4 Random dispersion management

Existing terrestrial fiber-optic telecommunication networks are patchwork systems, which include links with very different lengths [16]. This practically important circumstance suggests to consider transmission of RZ pulses (quasi-solitons) in *random* DM systems. It was shown that VA applies to this case too [106]. Random-DM models of different types were considered in works [1] and [73], where local values of the GVD coefficient, rather than the fiber-segment lengths, are distributed randomly. Actually, search for robust RZ pulses in random nonlinear fiber-optic systems is an issue not only important to the applications, but also fundamentally significant to the general theory of nonlinear waves in disordered media [96].

The basic equation and normalizations for the DM system with random distribution of the cell lengths can be taken in the same form as in the previous section, i.e., as per Eqs. (2.20), (2.21), and (2.22), with a difference that, in the random system, the normalizations must be applied to mean values of the randomly varying lengths. The consideration is limited here to the most important case when the lengths of the segments with the anomalous and normal GVD are equal in each DM cell, $L_1 = L_2 \equiv L/2$. Then, Eqs. (2.22) yield the mean values $\bar{L}_{1,2} = 1/2$, and $|\beta_{1,2} - \beta_0| = 2$. To comply with the former condition, one may assume that the random lengths are distributed uniformly in the interval

$$0.1 < L/2 < 0.9. \quad (2.32)$$

The minimum length 0.1 is introduced because, in reality, the length can be neither very large (say, larger than 200 km) nor very small (shorter than 20 km).

The same ansatz (2.23) and variational equations (2.26) and (2.27) which was applied above to the regular (periodic) DM system, may be used with its random counterpart. As explained above, the change of the soliton's parameters, $W_0 \rightarrow W_0 + \delta W_0$, $B_0 \rightarrow B_0 + \delta B_0$, within one DM cell is small. Therefore, the evolution of the pulse passing many cells may be approximated by smoothed differential equations,

$$\frac{dW_0}{dz} = \frac{\delta W_0}{\bar{L}^{(n)}}, \quad \frac{dB_0}{dz} = \frac{\delta B_0}{\bar{L}^{(n)}} \quad (2.33)$$

(n is the cell's number). Finally, the equations take the following form,

$$\frac{dW_0}{dz} = \frac{\sqrt{2}EW_0^4}{4L(z)} \left[\frac{1}{\sqrt{W_0^4 + 4B_0^2}} - \frac{1}{\sqrt{W_0^4 + 4(B_0 - L(z))^2}} \right], \quad (2.34)$$

$$\begin{aligned} \frac{dB_0}{dz} = & \beta_0 + \frac{\sqrt{2}EW_0^3}{8L(z)} \left[\frac{4B_0}{\sqrt{W_0^4 + 4B_0^2}} - \frac{4(B_0 - L)}{\sqrt{W_0^4 + 4(B_0 - L(z))^2}} \right. \\ & \left. + \ln \left(\frac{\sqrt{W_0^4 + 4B_0^2} - 2B_0}{\sqrt{W_0^4 + 4(B_0 - L(z))^2} - 2(B_0 - L(z))} \right) \right], \end{aligned} \quad (2.35)$$

where $L(z)$ is regarded as a continuous random function with values uniformly distributed in the interval (2.32).

The most essential characteristic of the pulse propagation at given values of β_0 and E is the cell-average pulse's width,

$$\bar{W} \equiv L^{-1} \int_{\text{cell}} W(z) dz. \quad (2.36)$$

Simulations of Eqs. (2.34) and (2.35) reveal that there are two drastically different dynamical regimes. If the soliton's energy is sufficiently small (hence the approximation outlined in the previous section is relevant) and PAD is anomalous or zero, i.e., $\beta_0 \leq 0$ (especially, if $\beta_0 = 0$), the pulse performs random vibrations but remains truly stable over long propagation distances. In the case when the energy is larger, as well as when PAD is normal, $\beta_0 > 0$, the pulse suffers fast degradation.

Following work [106], typical examples of the propagation are displayed in Fig. 2.7 for the zero-PAD case, which is the best one in terms of the soliton stability. Simulations of Eqs. (2.34) and (2.35) were performed with 200 different realizations of the random function $L(z)$. Figure 2.7 displays the evolution of $\langle \bar{W}(z) \rangle$, i.e., mean value of the width (2.36) averaged over the 200 random realizations, along with the corresponding normal deviations from the mean value. The figure demonstrates that some systematic slow evolution takes place on top of the random vibrations, which are eliminated by averaging over 200 realizations. Systematic degradation (broadening) of the soliton takes place too, but it is extremely slow if the energy is small. In the case shown in the bottom part of Fig. 2.7, the pulse survives, with very little degradation, the transmission through more than 1000 average cell lengths (in fact, as long as the simulations could be run). It is not difficult to understand this: in the limit of zero power, i.e., in the linear random-DM model, an exact solution for the pulse is available in an essentially the same form as given above for the periodic DM, see Eq. (2.23). If PAD is exactly zero, this exact solution predicts no systematic broadening of the pulse.

If the soliton's energy is larger, further simulations of Eqs. (2.34) and (2.35) show that, after having passed a very large distance, the slow spreading out of the soliton suddenly ends up with its blowup (complete decay into radiation). This seems to be qualitatively similar to what was predicted by the VA in the case of the periodic sinusoidal modulation of the dispersion, as shown in Fig. 2.2: a long sequence of chaotic

but nevertheless quasi-stable vibrations is suddenly changed by rapid irreversible decay.

In fact, the case of $\beta_0 = 0$ is a point of a *sharp optimum* for the random-DM system: at any finite anomalous PAD, $\beta_0 < 0$, the degradation of the pulses is essentially faster, especially for pulses with larger energy, and at any small normal value of PAD, $\beta_0 > 0$, very rapid decay always takes place, virtually at all values of the energy.

Comparison of the results predicted by VA with direct simulations of the full random-DM model was also reported in work [106]. Direct numerical results, averaged over the same number (200) of the realizations of the random-length set $L^{(n)}$, turn out to be quite similar to what was predicted by VA. In particular, the most stable propagation is again observed at zero PAD, the soliton's broadening is faster at nonzero anomalous PAD, and all solitons decay very quickly at nonzero normal PAD. The soliton's stability in direct simulations drastically deteriorates with the increase of the energy, as was also predicted by the VA.

Detailed comparison shows that, surprisingly, direct simulations yield somewhat *better* results for the soliton's stability than the VA: the actual broadening rate of the soliton may be $\sim 20\%$ smaller than that predicted by VA. The slow long-scale oscillations, clearly seen in Fig. 2.7, are less pronounced in direct simulations. The sudden decay into radiation, predicted by the VA after very long propagation, is not observed in direct simulations; instead, the soliton eventually splits into two smaller ones, quite similar to what is observed in direct simulations of the model with the periodically modulated dispersion, see Fig. 2.4.

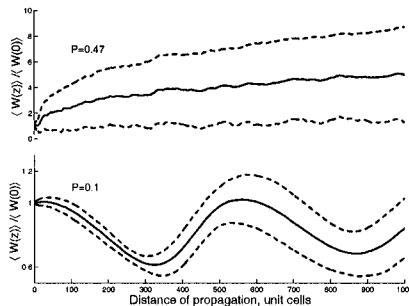


Figure 2.7: Evolution of the cell-average pulse width in the random-DM system with zero path-average dispersion, as predicted by the variational approximation. The propagation distance exceeds 1000 DM cells. The top and bottom panels correspond, respectively, to high and low power, $P = 0.47$ and $P = 0.1$. The mean values (solid curve) and standard deviations from them (dashed curves) are produced by numerical integration of equations (2.34) and (2.35), followed by averaging over 200 different realizations of the random length set.

To conclude this section, it is relevant to mention that some other versions of the DM systems, also different from strictly periodic ones, were studied too. In particular, an interesting possibility is to consider the so-called “hyperbolic” model, in which the size of the DM cell is fixed, while the PAD gradually decreases, as $1/z$, with the

propagation distance (which is achieved by a slow systematic change of the ratio of the anomalous- and normal-GVD segments in the DM map). It was demonstrated that the system of the latter type is especially efficient in suppressing the soliton's jitter [178].

2.5 Dispersion-managed solitons in the system with loss, gain and filtering

As mentioned above, a strong incentive for the introduction of the DM schemes for solitons was the potential that they offer for suppression of the jitter induced by the optical noise in the fiber through the Gordon-Haus effect. However, the DM alone cannot provide for complete suppression of the jitter, that is why long-haul dispersion-managed links for the transmission of solitons must include optical bandpass filters [120] (the filters are well known to be a versatile tool of the jitter control [16]). Therefore, it is necessary to modify the theory outlined above, in order to take the filtering into regard. Simultaneously, a model of the real-world fiber-optic link must include fiber loss and compensating gain provided by linear amplifiers periodically inserted into the link (these very amplifiers are also the main source of the optical noise that gives rise to the jitter). In this section, basic results for solitons in the filtered DM model will be presented, following the analysis developed in works [32] and [40]. A qualitative difference from the results outlined above for the lossless model is that there is a minimum value of the pulse's peak power necessary for the existence of stable solitons.

2.5.1 Distributed-filtering approximation

In the most typical case, the characteristic soliton period z_{sol} in long-haul fiber links (see Eq. (1.16) for the definition of z_{sol}) is quite large, $\sim 200 - 300$ km, while the spacing between the amplifiers is essentially smaller, $\sim 50 - 80$ km. Normally, bandpass filters are integrated with amplifiers, therefore the spacing between the filters is relatively small too. This suggests to adopt the approximation in which the corresponding modified NLS equation (2.20) neglects the discrete placing of the amplifiers and filters, assuming that they are distributed uniformly along the link. The accordingly modified NLS equation takes the form

$$iu_z - \frac{1}{2}\beta(z)u_{\tau\tau} + \gamma|u|^2u = ig_0u + ig_1u_{\tau\tau}, \quad (2.37)$$

where $g_1 > 0$ is the effective filtering coefficient, and $g_0 > 0$ is gain necessary to compensate the filtering losses; the model implies that the fiber loss proper is compensated by the main part of the gain, that does not appear in Eq. (2.37) in the distributed-gain approximation. It is necessary to stress that, despite the use of the assumption postulating the uniformly distributed filtering and gain, the model based on Eq. (2.37) belongs to the general class of the periodic strongly inhomogeneous nonlinear systems, due to the presence of the DM on the left-hand side of the equation.

Following the lines of the analysis developed for the lossless model, one can treat the filtering and gain terms in Eq. (2.37) as additional small perturbations (which

completely corresponds to the realistic conditions in fiber-optic telecommunications). The perturbation theory may again be based on the ansatz (2.23), which, by itself, is the exact solution of Eq. (2.20) in the absence of the nonlinearity, filtering and gain. One can easily see that, in fact, the Gaussian ansatz provides for an *exact solution* to Eq. (2.37) if the nonlinearity is still neglected, while the linear terms on the right-hand side are taken into regard. The corresponding exact solution is obtained from (2.23) by the substitution

$$B(z) \rightarrow \tilde{B}(z) \equiv \int_0^z \beta(z') dz' + B_0 - ig_1 z, \quad P_0 \rightarrow P_0 e^{2g_0 z} \quad (2.38)$$

(note that the accumulated dispersion \tilde{B} , modified by the filtering, is complex).

Next, one can analyze conditions which single out established DM solitons, by demanding zero changes of parameters W_0 and B_0 after the passage of one DM map (recall these conditions result in Eqs. (2.29) in the lossless model). As follows from Eq. (2.38) and from the way the accumulated dispersion enters the Gaussian ansatz (2.23), the filtering and gain do not affect the evolution of B_0 , and generate an additional small change,

$$\Delta W_0 = 2g_1 L / W_0, \quad (2.39)$$

of the width parameter of the pulse passing the distance L corresponding to the DM map (the meaning of this result is quite simple: the filtering gives rise to spreading out of the pulse at a constant rate). A new condition, which is enforced by the filtering and gain terms, is that the energy of the pulse must also remain equal to the initial value after the passage of the DM map (in the conservative model, this condition holds automatically, provided that emission of linear “radiation” from the soliton may be neglected). To realize this additional condition, one should notice that the terms on the right-hand side of Eq. (2.37) give rise to the following exact evolution equation for the soliton’s energy E (which is defined as per Eq. (1.9)):

$$\frac{dE}{dz} \equiv \frac{d}{dz} \left(\frac{1}{2} \int_{-\infty}^{+\infty} |u(\tau)|^2 d\tau \right) = g_0 \int_{-\infty}^{+\infty} |u(\tau)|^2 d\tau - g_1 \int_{-\infty}^{+\infty} |u_\tau|^2 d\tau. \quad (2.40)$$

The substitution of the ansatz (2.23) into this equation and calculation of the integrals yields an explicit result for dE/dz , which can be further integrated over the interval $\Delta z = L$ corresponding to the DM-cell’s length. Finally, equating the energy change to zero yields a very simple relation which shows that the balance between the filtering loss and compensating gain uniquely selects the width parameter W_0 ,

$$W_0^2 = g_1 / g_0 \quad (2.41)$$

(which remained arbitrary without the filters [100]). Actually, Eq. (2.41) may be understood in a different way: for given W_0 , it determines the necessary value g_0 of the gain.

Amending the second relation in Eqs. (2.29) with regard to the filtering-induced change (2.39) of the width, and defining, for convenience, $\kappa \equiv \sqrt{2}/W_0$ and $\phi =$

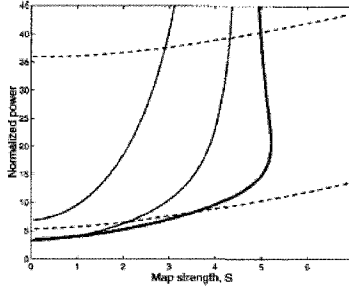


Figure 2.8: The diagram of the stationary transmission regimes for soliton in the DM model with filtering, as obtained from the analytically derived equations (2.42) and (2.43). The thin solid, bold solid, and dashed curves are reference lines which correspond, respectively, to the values $\beta_0/g_1 = -5$ and -1 (anomalous dispersion), $\beta_0/g_1 = 0$, and $\beta_0/g_1 = 1$ and 5 (normal dispersion).

$-2B_0/W_0^2$, the conditions for the pulse to be stationary are (the same normalizations (2.22) as in the lossless model are implied here)

$$\frac{\gamma P_0}{g_1} \left(\frac{1}{\sqrt{1+\phi^2}} - \frac{1}{\sqrt{1+(\phi+\kappa^2)^2}} \right) + \sqrt{2}\kappa^4 = 0, \quad (2.42)$$

$$\frac{\gamma P_0}{g_1} \left(\ln \left[\frac{\phi + \kappa^2 + \sqrt{1+(\phi+\kappa^2)^2}}{\phi + \sqrt{1+\phi^2}} \right] - \frac{2\kappa^2}{\sqrt{1+(\phi+\kappa^2)^2}} \right) - \sqrt{2} \left(\frac{\beta_0}{g_1} - 2\phi \right) \kappa^4 = 0. \quad (2.43)$$

(recall γ is the constant nonlinearity coefficient in Eq. (2.37)).

By solving Eqs. (2.42) and (2.43), one can find the dependence of the pulse's peak power P_0 on the pulse's width and *normalized* PAD, β_0/g_1 , in the presence of the filters. To facilitate the comparison with the lossless model (see Figs. 2.5), (2.6)), the results are displayed in Fig. 2.8 in terms of the map strength (2.25) and normalized peak power. Following work [32], the latter is taken as $0.22\gamma P_0 W_0^2/g_1$.

The results predicted by the analytical equations (2.42) and (2.43) are compared with results of direct numerical simulations in Fig. 2.9. Strictly speaking, the pulses in Eq. (2.37) are unstable because the gain term makes the trivial solution, $u = 0$, i.e., the background on which the soliton sits, unstable. Indeed, for high values of the gain, no stable solutions could be found numerically. Nevertheless, it is easy to find pulses that remain completely stable, at values of the parameters used in Fig. 2.9, after having passed, at least, 100 DM-map lengths, which is more than sufficient for the applications.

It is seen from the comparison of Figs. 2.8 and 2.9 that the analytical and numerical findings are in qualitative agreement. Further, comparing these figures to Figs. 2.5 and 2.6 which display analogous results for the lossless model, one notices a principally novel feature: the critical strength, $S_{cr} \approx 4$, which separates the stable transmission of

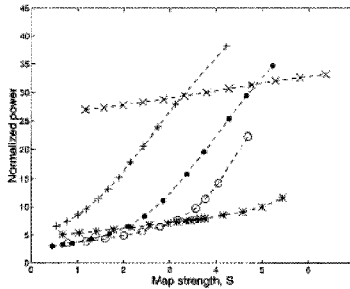


Figure 2.9: A counterpart of the diagram of stable soliton states shown in Fig. (2.8), as obtained from direct numerical simulations of Eq. (2.37), for $\beta_0/g_1 = -5$ ('+'), -1 (dot), 0 ('o'), 1 ('*') and 5 ('x').

the DM solitons at the anomalous and normal PAD, is removed, the stable transmission at zero and normal PAD being now possible at *any* map strength S . Instead, there appears, for the fixed filtering strength g_1 , a minimum (critical) power which is necessary for the stable transmission of the RZ pulses (solitons) in the filtered DM system. In particular, it was shown in work [32] that an absolute minimum of the normalized power, $\simeq 3.3$, is found for $S = 0$ and weakly anomalous PAD, $\beta_0/g_1 \simeq -0.7$.

The general conclusion (which is supported by more detailed numerical results [32]) is that the filtering makes the DM solitons essentially less sensitive to the exact value of PAD. This feature can be quite beneficial for the applications. In particular, in a multi-channel (WDM) system, the PAD may alter from a channel to a channel, because of the presence of the third-order dispersion in the fiber. The filtering will make the system more stable not only against the Gordon-Haus jitter, but also against the scatter of the PAD values.

2.5.2 The lumped-filtering system

The results obtained in the approximation of the uniformly distributed filtering and gain generally correctly describe qualitative properties of realistic systems with *lumped* (discretely placed) filters and amplifiers. Nevertheless, important features are missed by the distributed-filtering approximation – in particular, specific instability occurs if the filters are placed at “wrong” positions relative to the DM map, namely, at midpoints of the normal-GVD segments (while the transmission of the solitons is completely stable with the filters set at midpoints of the anomalous-DM segments) [121].

A full stability diagram for the DM solitons in the model with lumped amplifiers was recently obtained in work [40]. The model is based on Eq. (2.37), with the right-hand side replaced by the following lumped-filtering expression:

$$ig_0u + ig_1u_{\tau\tau} \rightarrow i \sum_n \delta(z - z_0 - Ln) (g_0u + \hat{G}u), \quad (2.44)$$

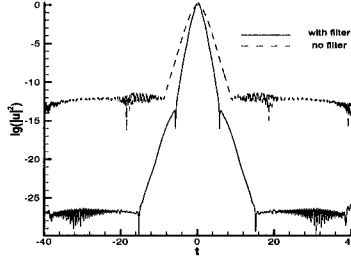


Figure 2.10: A typical example of the shape (shown on the logarithmic scale) of dispersion-managed solitons in the ideal lossless model, and in its realistic counterpart with lumped filters and amplifiers (for comparison, the solitons with equal amplitudes are taken in both cases). Each soliton is shown at a position (close to the midpoint of the anomalous-GVD segment of the DM map) where it is narrowest.

where the filtering operator \hat{G} is defined by its action on a temporal harmonic,

$$\hat{G}(e^{-i\omega\tau}) = -\left(\frac{\omega}{\Delta\omega}\right)e^{-i\omega\tau}, \quad \Delta\omega = \text{const} \quad (2.45)$$

(the latter is usually referred to as the Gaussian transfer function with the bandpass width $\Delta\omega$). A typical example of the shape of a stable soliton in this realistic model is shown (on the logarithmic scale of the power, which is relevant to display the soliton's shape) in Fig. 2.10; for comparison, the shape of the soliton in the lossless model, with the same DM map and the same value of the soliton's peak power, is also displayed in the figure. As is seen, a beneficial effect produced by the filters is suppression of the soliton's "wings", which is quite important to attenuate unwanted interactions between solitons carrying the data stream in a fiber-optic telecommunication link.

A full stability diagram for the DM solitons in this model was generated by means of numerical methods specially developed for this purpose in work [40]. The diagram is displayed in Fig. 2.11 (the stability borders shown in this figure are, actually, somewhat fuzzy, as, close to the borders, the RZ pulses observed in numerical simulations are still stable – in the sense that they do not decay – but they demonstrate irregular oscillations, and also change the shape, developing relatively large sidelobes attached to the main body of the soliton). Comparison of Figs. 2.11 and 2.9 shows that the distributed-filtering model indeed provides for a generally reasonable approximation to the lumped-filtering system.

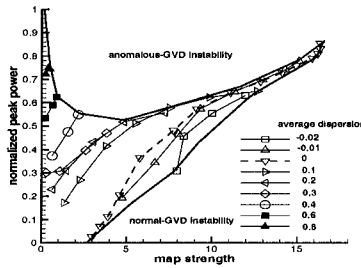


Figure 2.11: Stability diagram for the DM solitons in the realistic model with lumped filtering and amplification, given by Eqs. (2.37), (2.44), and (2.45). Symbol chains show stable solitons with different fixed values of the path-average dispersion (mean GVD). The overall stability area is bordered by the bold curves.

2.6 Collisions between solitons, and bound states of solitons in a two-channel dispersion-managed system

2.6.1 Effects of inter-channel collisions

The wavelength-division multiplexing (WDM), i.e., the use of a large number of data-bearing channels in the same fiber, carried by different wavelengths, is the most important direction in the development of optical telecommunications. In soliton-based systems, a serious problems posed by WDM is *crosstalk* due to collisions of pulses belonging to different channels. Collisions are inevitable, as the fiber's GVD gives rise to a difference in the group velocity (GVM) between the carrier waves in different channels.

In addition to the above-mentioned benefits of the jitter suppression in DM systems, another strong insensitive to study the soliton dynamics in DM systems is the fact the DM provides for strong suppression of the inter-channel crosstalk, as was first shown in direct simulations of a two-channel DM model reported in paper [134]. Besides that, collisions between solitons in coupled channels is a subject of considerable interest from the viewpoint of the general theory of solitons in periodic strongly inhomogeneous systems. In this section, an account of the analysis of collisions in the two-channel DM system will be given, following, chiefly, work [88].

The simplest two-channel system is described by two NLS equations coupled by the XPM (cross-phase-modulation) terms (cf. Eqs. (1.22) and (1.23)),

$$i(u_z + cu_\tau) - \frac{1}{2}\beta(z)u_{\tau\tau} + \left[-\frac{1}{2}\beta_0^{(u)}u_{\tau\tau} + \gamma(|v|^2 + 2|u|^2)u\right] = 0, \quad (2.46)$$

$$i(v_z - cv_\tau) - \frac{1}{2}\beta(z)v_{\tau\tau} + \left[-\frac{1}{2}\beta_0^{(v)}v_{\tau\tau} + \gamma(|u|^2 + 2|v|^2)v\right] = 0, \quad (2.47)$$

where $2c$ is the inverse-group-velocity difference between the channels (i.e., the GVM), $\beta(z)$ is the main part of the dispersion, with the zero average, that may be assumed the same in both channels, $\beta_0^{(u,v)}$ are values of the PAD in the channels, which are, generally, different. The nonlinear terms in Eqs. (2.46) and (2.47) represent the SPM and XPM effects.

An analytical approach to the problem may be based on the ansatz of the type (2.23) for the soliton in each channel, modified with regard to the inverse-group-velocity shifts $\pm c$ in Eqs. (2.46) and (2.47). In order to describe the dynamics of the interacting pulses, the ansatz should be further modified by applying independent Galilean boosts to u and v (cf. the boost formula (1.6) for $\beta = \text{const}$):

$$\begin{aligned} u(z, \tau; \omega) &= u_{\text{RZ}}^{(\text{linear})}(z, \tau - cz - T_u(z)) \exp[-i\omega_u \tau + i\psi_u(z)], \\ v(z, \tau; \omega) &= u_{\text{RZ}}^{(\text{linear})}(z, \tau + cz - T_v(z)) \exp[-i\omega_v \tau + i\psi_v(z)]. \end{aligned} \quad (2.48)$$

Here, ω_u and ω_v are frequency shifts of the two solitons, and the corresponding position shifts obey the equations

$$\frac{dT_u}{dz} = \omega_u [\beta(z) + \beta_0^{(u)}], \quad \frac{dT_v}{dz} = \omega_v [\beta(z) + \beta_0^{(v)}]. \quad (2.49)$$

In the absence of the interaction, parameters of the DM solitons in both channels are selected by the conditions (2.29). Since these conditions were obtained by treating the SPM nonlinearity as a small perturbation, the XPM-induced interaction between solitons may also be considered as another perturbation. This approach makes it possible to derive (by means of the Lagrangian technique, as shown in detail in work [88]) the following XPM-induced evolution equations for the frequency shifts of the solitons in the u - and v -channels:

$$\frac{d}{dz} \begin{Bmatrix} \omega_u \\ \omega_v \end{Bmatrix} = \frac{2^{5/2} P_{v,u} W_0^4 cz}{[W_0^4 + 4B^2(z)]^{3/2}} \begin{Bmatrix} +P_v \\ -P_u \end{Bmatrix} \exp \left[-\frac{W_0^2 (\Delta T(z))^2}{W_0^4 + 4B^2(z)} \right], \quad (2.50)$$

where P_u and P_v are the peak powers of the pulse in the u - and v -channels, and $\Delta T(z)$ is the temporal separation between the solitons. According to *ansätze* (2.48) and Eqs. (2.49), $\Delta T(z)$ obeys the equation

$$\frac{d}{dz} \Delta T = 2c + \omega_u [\beta(z) + \beta_0^{(u)}] - \omega_v [\beta(z) + \beta_0^{(v)}]. \quad (2.51)$$

The dynamical equations (2.50) are not only important for the application to optical telecommunications, but also help to understand the nature of the soliton's dynamics in the system: in the present approximation, the solitons may be regarded as quasi-particles with the coordinates T_u and T_v , if the evolution variable z is treated as formal time, $\omega_u + c$ and $\omega_v - c$ being momenta of the particles. In terms of this mechanical interpretation, $\beta(z) + \beta_0^{(u)}$ and $\beta(z) + \beta_0^{(v)}$ are proportional to the corresponding inverse masses (note that the DM solitons are characterized by the *time-dependent* effective masses, which periodically flip the sign), and Eq. (2.50) is a force of the interaction between the particles, which depends on the distance ΔT between them. In

this connection, it is relevant to mention that a dynamical equation similar to (2.50) was derived in work [10] for a two-channel model with constant GVD. However, there is a principal difference between the collisions in the two-channel DM system and in its constant-dispersion counterpart: as the coefficient $\beta(z)$ in Eqs. (2.49) periodically changes its sign (i.e., the effective masses periodically flip their sign, as mentioned above), in the strong-DM regime colliding pulses pass through each other *many times* before separating.

In the case relevant for the application to the WDM system in optical telecommunications, the term $2c$ in Eq. (2.51) is much larger than the two other terms [88], therefore Eq. (2.50) may be replaced by a simpler one, with

$$\Delta T(z) = 2cz \quad (2.52)$$

(however, a case is also possible when this assumption is not valid; then, the two solitons may form a *bound state* [63], see below).

It is necessary to distinguish between *complete* and *incomplete* collisions. In the former case, the solitons are far separated before the collision, while in the latter case, which corresponds to a situation when the collision occurs close to the input point ($z = 0$), the solitons begin the interaction being strongly overlapped. In either case, the most important result of the collision are shifts of the soliton's frequencies $\delta\omega_u$ and $\delta\omega_v$, which can be calculated as

$$\delta\omega_{u,v} = \int_{z_0}^{+\infty} \frac{d\omega_{u,v}}{dz} dz. \quad (2.53)$$

Here $d\omega_{u,v}/dz$ are to be taken from Eq. (2.50), with $\Delta T(z)$ replaced by $2cz$, as per Eq. (2.52). The lower limit of the integration in the expression (2.53) is finite for the incomplete collision, while the complete collision corresponds to $z_0 = -\infty$. The frequency shift is very detrimental in terms of the fiber-optic telecommunications, as, through the GVD, it gives rise to a change of the soliton's velocity. If the soliton picks up a "wrong" velocity, information carried by the soliton stream in the fiber-optic link may be completely lost.

An estimate of physical parameters for the *dense* WDM arrangements, with the actual wavelength separation between the channels $\delta\lambda < 1$ nm (this is the case of paramount practical interest) shows that, although the term $2c$ dominates in Eq. (2.51), c may be regarded as a small parameter in the integral expression (2.53), in the sense that the function cz varies slowly in comparison with the rapidly oscillating accumulated dispersion $B(z)$. In this case, the integral (2.53) and similar integrals can be calculated in a fully analytical form, as shown in work [88]. In particular, Eq. (2.53) yields *zero* net frequency shift for the complete collision, which shows the ability of the DM to suppress collision-induced effects. In fact, the zero net shift is a result of the multiple character of the collision (see above): each elementary collision generates a finite frequency shift, but they sum up to zero.

If the frequency shift is zero, the collision is characterized by a position shift, which is a detrimental effect too in optical telecommunications, but less dangerous than the

frequency shift. The position shift can be found from Eq. (2.49),

$$\delta T_{u,v} \equiv \int_{-\infty}^{+\infty} \frac{dT_{u,v}}{dz} dz = -\epsilon \beta_0^{(u,v)} \int_{-\infty}^{+\infty} z \frac{d\omega_{u,v}}{dz} dz - \int_{-\infty}^{+\infty} B(z) \frac{d\omega_{u,v}}{dz} dz, \quad (2.54)$$

where integration by parts was done. Then, substituting the expression (2.50) for $d\omega_{u,v}/dz$, one can perform the integrations analytically, to obtain a very simple final result:

$$\begin{Bmatrix} \delta T_u \\ \delta T_v \end{Bmatrix} = \frac{\sqrt{2\pi} W_0}{4c^2} \begin{Bmatrix} \beta_0^{(u)} P_v \\ \beta_0^{(u)} P_u \end{Bmatrix}. \quad (2.55)$$

This result contains a product of two small parameters, namely, the PAD $\beta_0^{(u,v)}$ and power $P_{v,u}$ (the latter is small as it measures the nonlinearity in the system, and it was assumed from the very beginning that the nonlinearity is a small perturbation).

The frequency shift generated by the incomplete collision can be found similarly. In this case, the worst (largest) result is obtained for the configuration with centers of the two solitons coinciding at the launching point $z = 0$:

$$(\delta\omega_{u,v})_{\max} = \frac{P_{v,u}}{\sqrt{2}cS} \ln \left(S + \sqrt{1 + S^2} \right), \quad (2.56)$$

where S is the DM strength defined by Eq. (2.25).

These analytical results were compared with numerical simulations. First of all, simulations show that the frequency shift generated by complete collisions is very small indeed (much smaller than in the case of incomplete collisions at the same values of parameters). As for the position shift in the case of the complete collision, the analytical prediction (2.55) for it is compared to numerical results in Fig. 2.12, showing a reasonably good agreement. In the case of incomplete collisions, simulations yield a nonzero frequency shift, which was compared to the analytical prediction (2.56) in work [88], also showing a reasonable agreement.

2.6.2 Inter-channel bound states

The case when the last two terms in Eq. (2.51) are comparable to $2c$ is relatively exotic but physically possible too. For this case, formation of *stable bound states* of two solitons belonging to the different channels was predicted in work [63]. In physical units, the “exotic” conditions mean that, for the wavelength separation between the channels ~ 0.1 nm, a large peak power of the solitons is needed, ~ 1 W. While this effect is not practically important in terms of optical telecommunications, it is interesting for the study of the soliton dynamics. These bound states were studied in work [63] by means of the VA and direct simulations. The former was actually based on Eqs. (2.50) and (2.51), without the simplifying assumption (2.52). It was found that VA predictions compare quite well with direct numerical results. Studied were both the symmetric system, with equal PADs in the two channels (zero, anomalous, or normal), and asymmetric ones, with zero PAD in one channel and either anomalous or normal

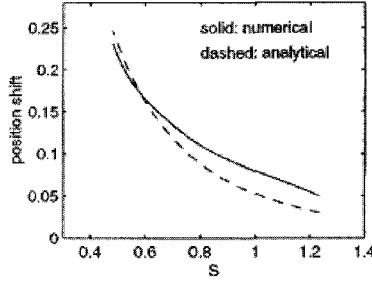


Figure 2.12: The analytically and numerically found position shift of the soliton induced by the complete collision in the two-channel DM model described by Eqs. (2.46) and (2.47) with $L_1 = 0.4$, $L_2 = 0.6$, $\beta_1 = -5/2$, $\beta_2 = 5/3$, $2c = 0.3$, peak powers of the colliding pulses being $P_u = P_v = 0.1$.

PAD in the other, or with opposite signs of the PADs in the two channels. In all the cases, it was found that stable bound states in which the solitons oscillate relative to each other exist indeed, provided that the energy of the solitons exceeds a certain minimum value E_{\min} , that depends on PADs and the inverse-group-velocity difference $2c$ between the channels. There is, however, a maximum value of $2c$, beyond which no bound state is possible. Typical examples of the dependences $E_{\max}(2c)$ are displayed in Fig. 2.13. Additionally, it was demonstrated in work [63] that, in the case when PAD in one channel is normal and so large that the DM soliton is unstable in it, the interaction with the soliton in the mate channel with anomalous PAD can produce a completely stable bound state.

2.6.3 Related problems

It is relevant to mention another two-channel model that, generally, also belongs to the class of the periodic heterogeneous nonlinear systems, although it does not involve DM. Instead, the group-velocity mismatch between the two XPM-coupled modes is subjected to periodic modulation, i.e., the model is based on the system of NLS equations (1.22), (1.23) with $\beta_u = \beta_v = \text{const} < 0$, $\gamma = \text{const} > 0$, $\sigma = 2$, and $c(z) = c_0 \sin(kz)$. A natural object in this model, considered in work [112], is a two-component symmetric soliton, with equal energies in both components. Without the modulation of $c(z)$, this compound soliton features an eigenmode of intrinsic excitation, in the form of mutual oscillations of centers of the two components, which was studied in detail [169, 87, 114]. The inclusion of the periodic modulation of the GVM between the components can give rise to resonant effects, if the modulation (spatial) frequency, $2\pi/k$, is commensurate with the eigenfrequency of the above-mentioned intrinsic mode. This possibility was explored in work [112], although only in the framework of the VA (without direct simulations of the coupled NLS equations). It was shown that the periodic modulation of $c(z)$ may split the compound soliton into two free single-component ones, the minimum GVM-modulation amplitude, $(c_0)_{\min}$,

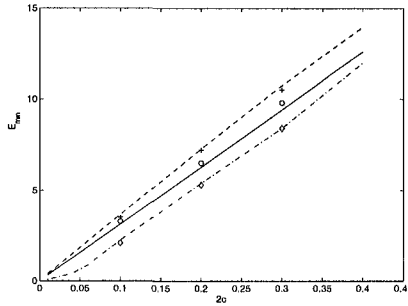


Figure 2.13: The minimum soliton's energy, necessary for the formation of bound states of solitons in the two-channel DM system, is shown as a function the inverse-group-velocity difference $2c$ for zero ($\beta_0^{(u)} = \beta_0^{(v)} = 0$), anomalous ($\beta_0^{(u)} = \beta_0^{(v)} = -0.1$), and normal ($\beta_0^{(u)} = \beta_0^{(v)} = 0.01$) path-average dispersion (PAD). The minimum energy predicted by the variational approximation for these three cases is shown, respectively, by solid, dashed-dotted, and dashed lines. Discrete symbols – circles, rhombuses, and crosses – represent values found from direct numerical simulations for the zero, anomalous, and normal PAD, respectively. The plots are aborted close to points where they abruptly shoot up (almost vertically); no bound state is possible for $2c > 0.40$ in the cases of the zero and normal PAD, and for $2c > 0.45$ with the anomalous PAD. In the asymmetric model, with $\beta_0^{(u)} \neq \beta_0^{(v)}$, the dependences $E_{\max}(2c)$ are quite similar.

necessary for the splitting, having deep minima (if considered as a function of k) at k corresponding to the fundamental and additional resonances with the intrinsic mode.

Interaction between DM solitons belonging to the same channel is also a problem of great interest (it is just “interaction”, rather than collision, as the solitons keep a relatively large separation between themselves, the interaction being mediated by “tails” of each soliton overlapping with neighboring ones). In fact, it was found that this kind of the interaction gives rise to the most serious factor limiting the use of the DM, as, for relatively strong DM ($S \gtrsim 2.5$), interaction effects severely affect the maximum distance of the error-free transmission of data by soliton streams (see papers [171, 146] and references therein). The source of the problem is that, in the strong-DM regime, the solitons periodically spread out, which leads, through their overlapping and resulting formation of “ghost” pulses, to accumulation of mutual distortion induced by the FWM effect [116]. Semi-analytical consideration of the intra-channel interactions between DM solitons, based on a specially devised version of VA, was worked out and yielded quite accurate results (as compared to direct simulations), but the analysis is cumbersome. Details can be found in work [171].



<http://www.springer.com/978-0-387-25635-1>

Soliton Management in Periodic Systems

Malomed, B.A.

2006, XII, 180 p. 78 illus., Hardcover

ISBN: 978-0-387-25635-1